

Journal of Biomedical Optics

BiomedicalOptics.SPIEDigitalLibrary.org

Dynamic near-infrared imaging reveals transient phototropic change in retinal rod photoreceptors

Rongwen Lu
Alexander M. Levy
Qiuxiang Zhang
Steven J. Pittler
Xincheng Yao

Dynamic near-infrared imaging reveals transient phototropic change in retinal rod photoreceptors

Rongwen Lu,^a Alexander M. Levy,^a Qiuxiang Zhang,^a Steven J. Pittler,^b and Xincheng Yao^{a,b}

^aUniversity of Alabama at Birmingham, Department of Biomedical Engineering, Birmingham, Alabama 35294

^bUniversity of Alabama at Birmingham, Department of Vision Sciences, Birmingham, Alabama 35294

Abstract. Stiles–Crawford effect (SCE) is exclusively observed in cone photoreceptors, but why the SCE is absent in rod photoreceptors is still a mystery. In this study, we employed dynamic near infrared light imaging to monitor photoreceptor kinetics in freshly isolated frog and mouse retinas stimulated by oblique visible light flashes. It was observed that retinal rods could rapidly (onset: ~10 ms for frog and 5 ms for mouse; time-to-peak: ~200 ms for frog and 30 ms for mouse) shift toward the direction of the visible light, which might quickly compensate for the loss of luminous efficiency due to oblique illumination. In contrast, such directional movement was negligible in retinal cones. Moreover, transient rod phototropism could contribute to characteristic intrinsic optical signal (IOS). We anticipate that further study of the transient rod phototropism may not only provide insight into better understanding of the nature of vision but also promise an IOS biomarker for functional mapping of rod physiology at high resolution. © The Authors. Published by SPIE under a Creative Commons Attribution 3.0 Unported License. Distribution or reproduction of this work in whole or in part requires full attribution of the original publication, including its DOI. [DOI: 10.1117/1.JBO.18.10.106013]

Keywords: Stiles–Crawford effect; phototropism; photoreceptor; directional illumination.

Paper 130548R received Jul. 31, 2013; revised manuscript received Oct. 1, 2013; accepted for publication Oct. 3, 2013; published online Oct. 28, 2013.

1 Introduction

The Stiles–Crawford effect (SCE) states that luminance efficiency is dependent on incident light direction relative to the eye axis.¹ It is well established that the retina is more sensitive to light entering the center of the pupil, i.e., parallel light relative to eye axis, than light passing through the periphery, i.e., oblique light illumination. The SCE is exclusively observed in cones, which can benefit good vision quality by suppressing intraocular stray light under photopic conditions.² In contrast, the SCE has not been detected in rods, which dominate scotopic vision.² In other words, the absorption efficiency of light by rods was not affected by the incident angle in early SCE studies which were performed with psychophysical methods.² The biophysical mechanisms underlying this rod/cone difference are not established. In this study, we conducted dynamic near infrared (NIR) light imaging to explore transient changes in rod and cone photoreceptors activated by oblique light stimuli. High-spatial (micrometers) and high-temporal (milliseconds) resolution NIR imaging revealed that 80% of rods could rapidly move toward the direction of oblique stimulus light while such directional movement was negligible in cones. Our experimental results suggest that transient phototropic adaptation may quickly compensate for the loss of luminous efficiency in rods activated by oblique stimulation, which can explain the absence of the SCE in the rod system. The observed transient phototropic adaptation of retinal rods not only provides insight into the nature of vision but also promises an intrinsic optical signal (IOS) biomarker. This would enable noninvasive, high-resolution assessment of rod function, which is known to be more vulnerable than cone function in aging and early age-related macular degeneration

(AMD),^{3,4} the most common cause of severe vision loss and legal blindness in adults over 50.^{3,5}

2 Materials and Methods

2.1 Retina Preparation

Animal handling was approved by the Institutional Animal Care and Use Committee of the University of Alabama at Birmingham. Both frog (*Rana pipiens*) and mouse (*Mus musculus*) retinas were used to demonstrate the transient phototropic adaptation in the retina.

Frog retinas were selected as primary specimens in this study for several reasons. First, the relatively large size of frog (compared to mouse or other mammalian) photoreceptors allows unambiguous observation of individual photoreceptors. Second, the diameter of frog rods (~5 to 8 μm) is much larger than cones (~1 to 3 μm),^{6,7} and thus, rod and cone photoreceptors can be easily separated based on their cellular diameters. Third, rod and cone numbers are roughly equal in frog retinas,^{6,7} and thus, unbiased analysis of rod and cone cells can be readily achieved. Preparation procedures of fresh living whole-mount frog retinas have been reported in previous publications.⁸ Briefly, the frog was euthanized by rapid decapitation and double pithing. After enucleating the intact eye, we hemisected the globe below the equator with fine scissors. The lens and anterior structures were removed before the retina was separated from the retinal pigment epithelium.

Mouse retinas were used to verify the transient phototropic adaptation in mammals. Five-month-old wild-type mice, which have been maintained for more than 20 generations from an original cross of C57Bl/6J to 129/SvEv, were used in this study. The *rd1* allele that segregated in the 129/SvEv stock was removed by genetic crossing and verified as previously described.⁹ Protocols for handling mouse samples were previously reported.¹⁰ Briefly, after the eyeball was enucleated

Address all correspondence to: Xincheng Yao, University of Alabama at Birmingham, Department of Biomedical Engineering, Birmingham, Alabama 35294. Tel: (205) 996-7459; Fax: (205) 934-3425; E-mail: xcy@uab.edu

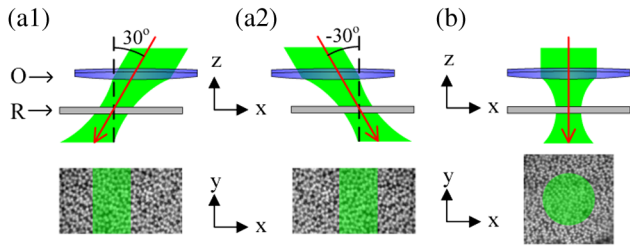


Fig. 1 Schematic diagram of stimulation patterns. O: objective; and R: retina. Black dash lines indicate the normal axis of retinal surface. Red solid lines indicate the incident directions. Top panels are cross-section view (transverse or x - z plane) and the bottom panels are enface view (axial or x - y plane). (a1) Rectangular stimulus (bottom panel) with 30-deg incident angle with respect to the normal axis of retinal surface (top panel). (a2) Rectangular stimulus (bottom panel) with -30-deg incident angle (top panel). (b) Circular stimulus (bottom panel) with 0-deg incident angle (top panel). The retina was placed with the ganglion cell layer facing toward the objective.

from anesthetized mice, the retina was isolated from the eyeball in Ames media and then transferred to a recording chamber. During the experiment, the sample was continuously superfused with oxygenated bicarbonate-buffered Ames medium, maintained at pH 7.4 and 33°C to 37°C.

2.2 Experimental Setup

The imaging system was based on a NIR digital microscope that has been previously used for functional imaging of living retinal tissues.¹⁰ A fast digital camera (Neo sCMOS, Andor Technology, Belfast, UK) with pixel size $6 \times 6 \mu\text{m}^2$ was used for retinal imaging. A 20 \times water immersion objective with 0.5 NA was used for frog experiments. Therefore, the lateral resolution of the system was about $1 \mu\text{m}$ ($0.61\lambda/\text{NA}$). For mouse experiments, we used a 40 \times water immersion objective with 0.75 NA which has the lateral resolution of $0.7 \mu\text{m}$. The system consisted of two light sources: a NIR (800 to 1000 nm) light for retinal imaging and a visible (450 to 650 nm) light-emitting diode (LED) for retinal stimulation. The duration of the visible flash was 5 ms. Figure 1 illustrates rectangular stimulus patterns with oblique incident angles [Fig. 1(a)] and a circular stimulus pattern with perpendicular incident angle [Fig. 1(b)]. Figures 1(a) and 1(b) were used for the experiments in Figs. 2 and 4, and Fig. 3, respectively. All images of retinas in this article were acquired at 200 frames/s.

2.3 Dynamic Calculation of Individual Photoreceptor Movements

In order to quantify transient phototropic changes in rod and cone systems, we calculated the displacement of individual

rods [Figs. 2(b) and 4(b)] and cones [Fig. 2(b)]. The level-set method¹¹ was used to identify the morphological edge of individual rods and cones. Then, the weight centroid was calculated dynamically, allowing accurate registration of the location of individual photoreceptors at nanometer resolution. The same strategy has been used in stochastic optical reconstruction microscopy¹² and photoactivated localization microscopy^{13,14} to achieve nanometer resolution to localize individual molecules with photoswitchable fluorescence probes. The three-sigma rule was used to set up a threshold to distinguish silent and active photoreceptors.¹⁰ If the stimulus-evoked photoreceptor shifted above this threshold, then this photoreceptor was defined as active. Otherwise, it was defined as silent. Thus, the active ratio of the rods and cones could be obtained [Fig. 2(c)].

2.4 Computer Algorithm of Localized Retinal Movements

The activated photoreceptors were displaced due to light stimulations [Figs. 2(c), 2(d), and 3(b)]. In order to quantify the photoreceptor displacements, the normalized cross correlation (NCC) between the poststimulus and prestimulus images was calculated to estimate localized retinal movements. We assume that $I_{ii}(x, y)$ was the image acquired at the time point of t_i , where $i = 1, 2, 3, \dots$ was the image index and (x, y) was the pixel position. We took the first image $I_{i1}(x, y)$ as the reference image. For the pixel at the position of (x_0, y_0) from the image I_{ii} , there would be a horizontal shift $H_{ii}(x_0, y_0)$ (parallel to the x axis) and a vertical shift $V_{ii}(x_0, y_0)$ (parallel to the y axis) compared to the reference image. At the position of (x_0, y_0) from the image I_{ii} , we took a subwindow W_{ii} ($m \times m$ pixels):

$$W_{ii}(x_0, y_0, u, v) = I_{ii}\left(x_0 - \frac{m-1}{2} + u, y_0 - \frac{m-1}{2} + v\right), \quad (1)$$

where $u = 1, 2, 3, \dots, m$ and $v = 1, 2, 3, \dots, m$. Here, we set $m = 13$ (corresponding to $3.9 \mu\text{m}$ at the retina). This window is at the level of individual cells (cone: 5 to $8 \mu\text{m}$ and rod: 1 to $3 \mu\text{m}$). We selected a corresponding subwindow of the reference image at the position of (x_1, y_1) :

$$W_{i1}(x_1, y_1, u, v) = I_{i1}\left(x_1 - \frac{m-1}{2} + u, y_1 - \frac{m-1}{2} + v\right). \quad (2)$$

Then the correlation coefficient could be calculated between two image matrices defined by Eqs. (1) and (2):

$$CC_{ii}(x_0, y_0, x_1, y_1) = \frac{\sum_{u=1}^m \sum_{v=1}^m [W_{ii}(x_0, y_0, u, v) - \overline{W_{ii}}][W_{i1}(x_1, y_1, u, v) - \overline{W_{i1}}]}{\left\{\sum_{u=1}^m \sum_{v=1}^m [W_{ii}(x_0, y_0, u, v) - \overline{W_{ii}}]\right\}^{0.5} \left\{\sum_{u=1}^m \sum_{v=1}^m [W_{i1}(x_1, y_1, u, v) - \overline{W_{i1}}]\right\}^{0.5}}, \quad (3)$$

where $\overline{W_{ii}}$ was the mean of the matrix $W_{ii}(x_0, y_0, u, v)$, and $\overline{W_{i1}}$ was the mean of the matrix $W_{i1}(x_1, y_1, u, v)$. We searched x_1 from $x_0 - k$ to $x_0 + k$, and y_1 from $y_0 - k$ to $y_0 + k$, where k was the searching size, set to be 3 (corresponding to $0.9 \mu\text{m}$ at the retina) here. Thus, we

could find the position $(x_{1\text{max}}, y_{1\text{max}})$, where the value of correlation coefficient defined by Eq. (3) was maximum. Therefore, the horizontal shift (parallel to x axis) and vertical shift (parallel to y axis) at the position (x_0, y_0) were obtained as:

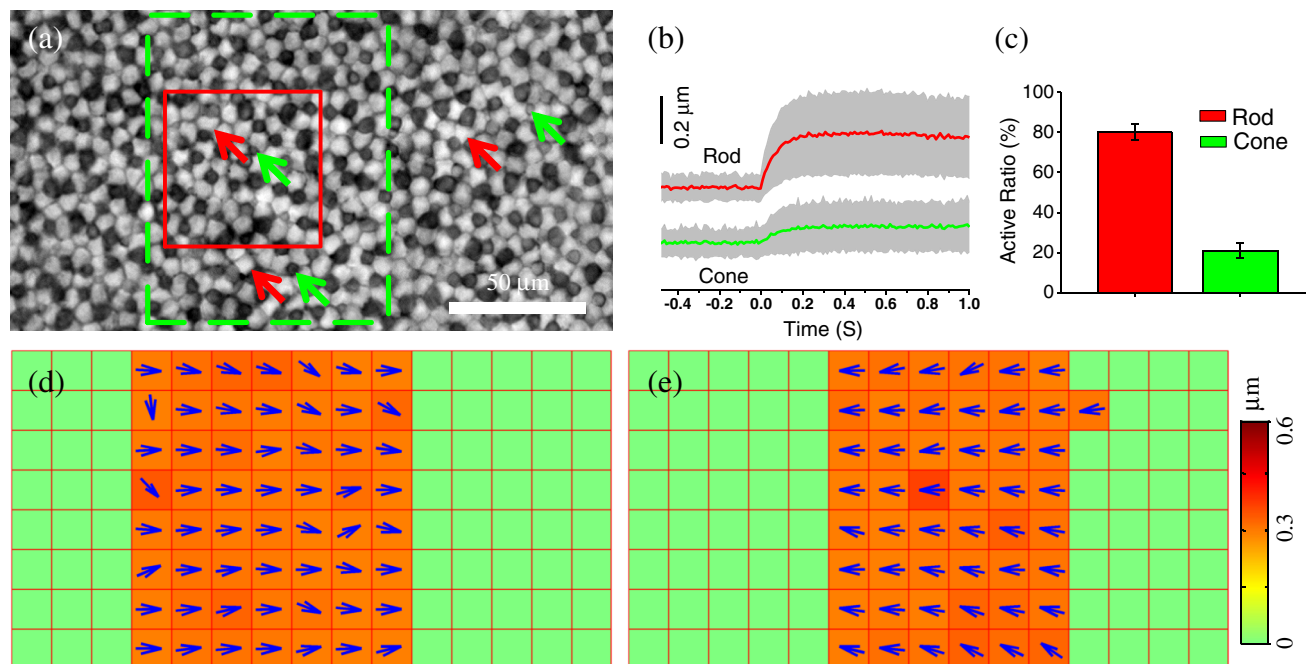


Fig. 2 Oblique stimulus-evoked photoreceptor displacements. (a) Near infrared (NIR) image of frog photoreceptor mosaic pattern. Green dashed window illustrates stimulus area. Red rectangle indicates the area shown in Video 1 (QuickTime, 7.7 MB) [URL: <http://dx.doi.org/10.1117/1.JBO.18.10.106013.1>] which displays a pair of pre- and poststimulus images alternating repeatedly 20 times. Red and green arrows point to rods and cones, respectively. (b) Average displacement of 25 rods and cones which were randomly selected from the stimulus area. The gray shadow indicates the standard deviation. (c) Active ratios of rods and cones at time 200 ms after the onset of the stimulus. Six trials were used. For each trial, 25 rods and cones were randomly selected. Thus, in each trial, the active ratio was calculated as the number of active rods or cones divided by 25. (d) Retinal displacements associated with the 30-deg stimulus [Fig. 1(a1)] at 200 ms. Dynamic changes of retinal displacement maps from -200 to 1000 ms are displayed in Video 2 (QuickTime, 6.7 MB) [URL: <http://dx.doi.org/10.1117/1.JBO.18.10.106013.2>]. (e) Retinal displacements associated with the -30 -deg stimulus [Fig. 1(a2)] at 200 ms. Each square in (d) and (e) represents a $15 \times 15 \mu\text{m}^2$ area of the retina. Transient displacements within the small square were averaged.

$$H_{ii}(x_0, y_0) = x_0 - x_{1 \max}, \quad (4)$$

$$V_{ii}(x_0, y_0) = y_0 - y_{1 \max}. \quad (5)$$

They could be rewritten as a complex number

$$H_{ii} + jV_{ii} = A_{ii} \exp(j\Phi_{ii}), \quad (6)$$

where j is the imaginary unit, A_{ii} is the shift amplitude map [the color images in Figs. 2(d), 2(e), and 3(b)] and Φ_{ii} is the direction map [directions of arrows in Figs. 2(d), 2(e), and 3(b)].

If

$$A_{ii}(x_0, y_0) \neq 0, \quad (7)$$

then the pixel (x_0, y_0) was displaced, thus defined as active. Therefore, the active pixel numbers could be plotted as a function of the time [Fig. 3(f)].

2.5 IOS Data Processing

In order to test the effect of the phototropic adaptation on the IOS pattern associated with circular stimulus, representative IOS images are illustrated in Fig. 3(c), with a unit of $\Delta I/I$, where I is the background light intensity and ΔI reflects the light intensity change corresponding to retinal stimulation. Basic procedures of IOS data processing have been previously reported.⁸

3 Results

3.1 Transient Phototropic Adaptation in Frog Retina Activated by Oblique Stimulation

Figure 2 shows results of phototropic adaptation correlated with oblique light stimulation. Figure 2(a) shows the photoreceptor mosaic pattern. Individual rods [red arrows in Fig. 2(a)] and cones [green arrows in Fig. 2(a)] could be observed. A rectangular stimulus with a 30 deg incident angle [Fig. 1(a1)] was delivered to the retina. Within the stimulation area, photoreceptor displacements were directly observed in NIR images (Video 1).

In order to quantify transient phototropic changes in rod and cone systems, we calculated displacements of individual rods and cones (see Sec. 2). Figure 2(b) shows average displacements of 25 rods and cones randomly selected from the stimulus window. The displacement of rods occurred almost immediately (<10 ms) and reached a magnitude peak at ~ 200 ms. The magnitude of rod displacement (average: $0.2 \mu\text{m}$, with maximum up to $0.6 \mu\text{m}$) was significantly larger than that of cone displacement (average: $0.048 \mu\text{m}$, with maximum of $0.15 \mu\text{m}$). In addition, as shown in Fig. 2(c), the active ratio (see Sec. 2 for definition) of rods was $80\% \pm 4\%$, while $20\% \pm 4\%$ of cones were activated. The observation indicated that the transient phototropic displacement was dominantly observed in rods.

In order to verify directional dependency of the phototropic adaptation, we used template matching with the NCC to compute nonuniform motion in the retina (see Sec. 2).¹⁵ As shown in

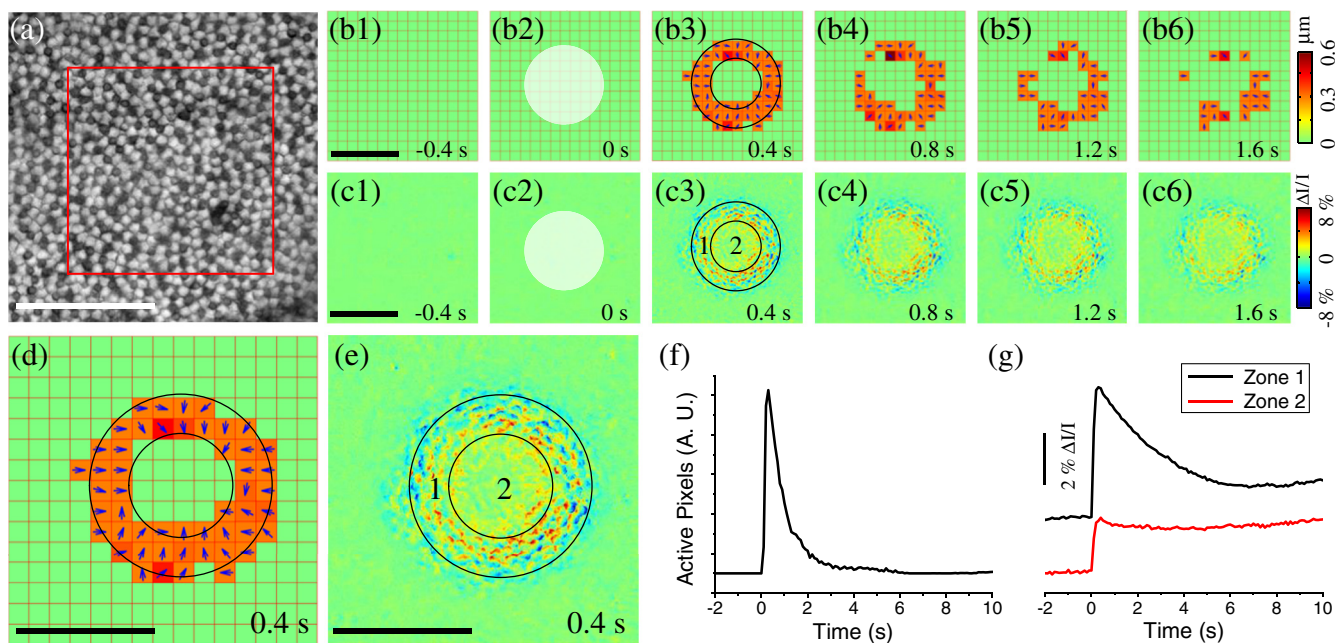


Fig. 3 Photoreceptor displacements and intrinsic optical signal (IOS) responses stimulated by circular stimulus (in transverse plane) with a Gaussian profile (in axial plane). (a) NIR image of frog photoreceptor mosaic. Red rectangle indicated the area shown in Video 3 (QuickTime, 7.9 MB) [URL: <http://dx.doi.org/10.1117/1.JBO.18.10.106013.3>] which displays a pair of pre- and poststimulus images alternating repeatedly 20 times. (b) Localized retinal displacements associated with circular stimulus. This stimulus had a Gaussian profile in axial plane [Fig. 1(b)]. The same methods as those in Figs. 2(e) and 2(f) were used here to produce the displacement maps. (c) IOS maps. ΔI reflected the light intensity change and I was the background light intensity. Zone 1 corresponds to the area within the inner ring. Zone 2 corresponds to the annular area. The stimulus was delivered at time 0. (d) Enlarged view of b3. (e) Enlarged view of c3. Scale bars indicate $100 \mu\text{m}$. (f) Dynamic change of the number of active pixels in (b). The pixel with nonzero value was defined as active. (g) Temporal IOS profiles.

Video 2 and Fig. 2(d), the stimulus-activated retina shifted to right, i.e., toward the direction of the 30-deg oblique stimulation. In order to confirm the reliability of the phototropic response, the incident angle of the stimulus was switched to -30 deg [Fig. 1(a2)], 5 min after the recording illustrated in Fig. 2(d). Figure 2(e) illustrates the transient movement corresponding to -30 deg stimulus at the same retinal area shown in Fig. 2(d). It was observed that the stimulated retina shifted toward the left [Fig. 2(e)], i.e., in the opposite direction compared to Fig. 2(d). Comparative recording of the 30 and -30 deg stimuli verified that transient photoreceptor movement was tightly dependent on the incident direction of the stimulus light.

3.2 Transient Phototropic Adaptation in Frog Retina Activated Oblique Stimulation by Circular (Transverse) Stimulation with a Gaussian (Axial) Profile

In addition to the aforementioned oblique stimulation, Fig. 3 shows transient photoreceptor displacements activated by a perpendicular circular stimulus with a Gaussian profile in the axial plane [Fig. 1(b)]. The circular aperture was conjugate to the focal plane of the imaging system. It is well known that cones taper toward the outer segment (OS) and are shorter than rods,⁶ which implies that the OS pattern should have relatively larger extracellular space between photoreceptors when compared to the inner segment (IS) pattern. Therefore, when the tight mosaic pattern of photoreceptors [Fig. 2(a)] was clearly observed, the focal plane was around the photoreceptor IS. Hence, at the more distal position, i.e., the OS, the stimulus light was divergent and became oblique at the edge. However, at the

central area, the stimulus light impinged the photoreceptor without directional dependence. Under this condition, only photoreceptors at the periphery of the stimulus pattern underwent displacement, which can be directly visualized in Video 3. Figures 3(b) and 3(d) not only confirmed this phenomenon but also revealed that peripheral photoreceptors shifted toward the center. The number of active pixels [see Eq. (7)] was plotted over time in Fig. 3(f). The rapid displacement occurred almost immediately (< 10 ms) after the stimulus delivery, reached the magnitude peak at ~ 200 ms, and recovered at ~ 2 s. It was consistently observed that the stimulus-evoked displacement was rod dominant. Utilizing the same methods employed in Fig. 2(c), rod and cone displacements were quantitatively calculated. Within the annular area in Fig. 3(d), 25 rods and cones were randomly selected for quantitative comparison. $74\% \pm 6\%$ of rods were activated, whereas $24\% \pm 5\%$ of cones were activated at 200 ms after the onset of stimulus (six samples).

3.3 Correlation of Transient Phototropism and IOS in Frog Retina

We speculated that the transient phototropic changes may partially contribute to stimulus-evoked IOSs, which promised a noninvasive method for spatiotemporal mapping of retinal function.^{8,16} IOS images shown in Fig. 3(c) confirmed the effect of IOS enhancement at the edge of the circular stimulus. The edge-enhanced IOS response gradually degraded over time, which was consistent with the change of the photoreceptor displacement [Fig. 3(b)]. In addition, both positive and negative IOS signals, with high magnitude, were observed at the periphery of the stimulus pattern. In contrast, the IOS signal at the stimulus center [Zone 2, Fig. 3(e)] was positive dominant, and the IOS

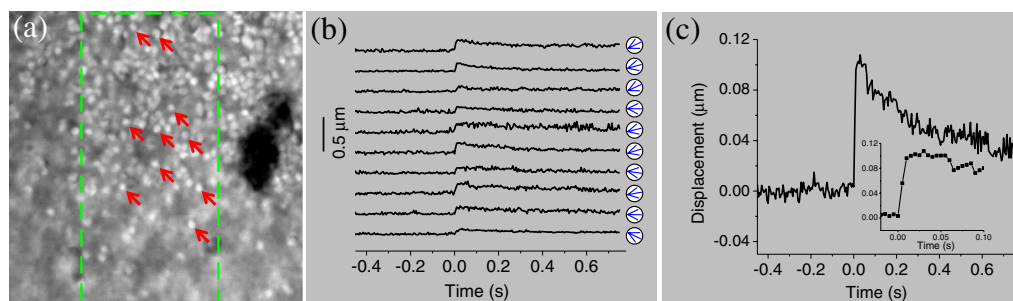


Fig. 4 Stimulus-evoked photoreceptor displacements at the mouse retina. (a) NIR image of mouse photoreceptor mosaic. A 40 \times objective with 0.75 NA was used. The image size corresponds to a $60 \times 60 \mu\text{m}^2$ area at the retina. The green dashed rectangle indicates the oblique stimulation area. (b) Displacements of 10 photoreceptors over time. The stimulus was delivered at time 0. These 10 photoreceptors were specified by arrows in (a). Green arrows in circles indicate the direction of the displacement at time 30 ms after stimulation. (c) Averaged displacement of 10 photoreceptors. The inset panel shows the same data within the time period from -0.02 to 0.1 s.

magnitude was weaker than that observed at peripheral area [Zone 1, Fig. 3(e)]. Moreover, time courses of IOS responses were different between Zone 1 and Zone 2 [Fig. 3(g)]. The central IOS curve [black curve in Fig. 3(g)] more resembled the curve of the active pixel number [Fig. 3(f)], which suggested that transient phototropic change primarily contributes to the periphery IOSs.

3.4 Transient Phototropic Adaptation in Mouse Retina Activated by Oblique Stimulation

In order to verify the transient phototropic changes in mammals, we have conducted a preliminary study of mouse retinas with oblique stimulation. Unlike large frog photoreceptors (rod: ~ 5 to $8 \mu\text{m}$, cone: ~ 1 to $3 \mu\text{m}$), mouse photoreceptors (1 to $2 \mu\text{m}$ for both rods and cones) are relatively small.^{17,18} Although individual mouse photoreceptors [Fig. 4(a)] were not as clear as frog photoreceptors [Figs. 2(a) and 3(a)], we selected representative individual mouse photoreceptors [arrows in Fig. 4(a)], which could be unambiguously isolated from others. Figure 4(b) shows temporal displacements of 10 mouse photoreceptors pointed out in Fig. 4(a). These 10 photoreceptors shifted to the left [arrows in Fig. 4(b)]. Figure 4(c) shows an average magnitude of photoreceptor displacements. As shown in Fig. 4(c), the displacement occurred within 5 ms and reached the peak at 30 ms.

4 Discussion

In summary, high-spatial and temporal-resolution imaging revealed rod-dominant transient phototropic response in frog (Fig. 2) and mouse (Fig. 4) retinas under oblique stimuli. Such transient phototropic response could compensate for the loss of illumination efficiency under oblique stimulation in the rod system. Although the image resolution in Fig. 4(a) was not high enough to separate rods and cones reliably, we speculate that the observed displacement was rod dominated due to the established knowledge that rods account for $\sim 97\%$ of total number of the photoreceptors in mouse retinas.¹⁹ In contrast to rods, it can take a long time, at least tens of seconds or even days, for cone adaptation.²⁰ In other words, rapid (onset: ~ 10 ms for frog and ~ 5 ms for mouse; time-to-peak: ~ 200 ms for frog and ~ 20 ms for mouse) phototropic adaptation in retinal rods is too quick for the SCE to be detected by conventional psychophysical methods with the advanced involvement of brain perception. Gaussian-shape stimulation further confirmed the transient rod displacement (Fig. 3). In addition, the observed off-center and on-

surround pattern [Fig. 3(b)] may imply early involvement of the photoreceptors in contrast enhancement. The edge enhancement was confirmed by the IOS maps [Fig. 3(c)]. In general, it is believed that the center-surround antagonism, which is valuable for contrast perception, is initiated by horizontal cells^{21,22} and/or amacrine cells.²³ However, our experimental results here suggest that the discrepancy of the incident angle between the surround and the center of the Gaussian illumination [Fig. 1(b)] can evoke directional displacement only at the surround [Fig. 3(b)]. Such an edge-enhanced pattern of photoreceptor activity may suggest an early involvement of the photoreceptors in contrast perception.

Moreover, the observed transient rod movement provides an IOS biomarker to allow early detection of eye diseases that can cause retinal dysfunction. Rod function has been well established to be more vulnerable than cones in aging and early AMD,^{3,4} which is the most common cause of severe vision loss and legal blindness in adults over 50.^{3,5} Structural biomarkers, such as drusen and pigmentary abnormalities in the macula, are important for retinal evaluation. Adaptive optics imaging of individual rods has been recently demonstrated.^{24–26} However, the most commonly used tool for retinal imaging, the fundus examination, is not sufficient for a final retinal diagnosis.²⁷ In principle, physiological function is degraded in diseased cells before detectable abnormality of retinal morphology. Psychophysical methods^{28–30} and electroretinography³¹ measurements have been explored for functional assessment of the retina, but reliable identification of localized rod dysfunctions is still challenging due to limited resolution and sensitivity. The experimental results shown in Fig. 3 indicate that the transient phototropic changes can partially contribute to IOS recording, which has the potential to be developed into a superior noninvasive method for spatiotemporal mapping of retinal function.^{8,10} The different time courses of the IOSs at Zone 1 (periphery) and Zone 2 (center) suggest that the phototropic change of rod photoreceptors primarily contributes to the periphery IOS response. Multiple IOS origins, including neurotransmitter secretion,³² refractive index change of neural tissues,³³ interactions between photoexcited rhodopsin and guanosine triphosphate (GTP)-binding protein,³⁴ disc shape change,³⁵ cell swelling,³⁶ etc., have been proposed. In order to investigate the biophysical mechanism of transient phototropic adaptation, we are currently pursuing optical coherence tomography of retinal photoreceptors to quantify the axial location of phototropic kinetics. Further investigations are also planned to quantify time courses of the transient phototropic adaptations in wild type and

diseased mouse retinas. We anticipate that further investigation of the rod-dominant phototropic effect can provide a high-resolution methodology to achieve objective identification of rod dysfunction, thereby allowing early detection and easy treatment evaluation of eye diseases, such as AMD-associated photoreceptor degeneration.

Acknowledgments

This research is supported in part by NSF CBET-1055889, NIH R21 EB012264, UASOM I3 Pilot Award and NEI R01 EY018143-05. The authors wish to thank Dr. Christine Curcio and Dr. Walter Makous for their valuable comments and constructive suggestions on the manuscript, we thank Delores W. Davis in Dr. Pittler's laboratory for providing the mice and relevant genotype and age information.

References

1. W. S. Stiles and B. H. Crawford, "The luminous efficiency of rays entering the eye pupil at different points," *Proc. R. Soc. Lond.* **112**(778), 428–450 (1933).
2. G. Westheimer, "Directional sensitivity of the retina: 75 years of Stiles-Crawford effect," *Proc. Biol. Sci.* **275**(1653), 2777–2786 (2008).
3. C. A. Curcio, N. E. Medeiros, and C. L. Millican, "Photoreceptor loss in age-related macular degeneration," *Invest. Ophthalmol. Vis. Sci.* **37**(7), 1236–1249 (1996).
4. C. Owsley et al., "Cone- and rod-mediated dark adaptation impairment in age-related maculopathy," *Ophthalmology* **114**(9), 1728–1735 (2007).
5. N. M. Bressler, S. B. Bressler, and S. L. Fine, "Age-related macular degeneration," *Surv. Ophthalmol.* **32**(6), 375–413 (1988).
6. S. E. Nilsson, "An Electron Microscopic Classification of the Retinal Receptors of the Leopard Frog (*Rana pipiens*)," *J. Ultrastruct. Res.* **10**(5), 390–416 (1964).
7. P. A. Liebman and G. Entine, "Visual pigments of frog and tadpole (*Rana pipiens*)," *Vis. Res.* **8**(7), 761–775 (1968).
8. X. C. Yao and Y. B. Zhao, "Optical dissection of stimulus-evoked retinal activation," *Opt. Express* **16**(17), 12446–12459 (2008).
9. S. J. Pittler and W. Baehr, "Identification of a nonsense mutation in the rod photoreceptor cGMP phosphodiesterase beta-subunit gene of the rd mouse," *Proc. Natl. Acad. Sci. U.S.A.* **88**(19), 8322–8326 (1991).
10. Q. X. Zhang et al., "Comparative intrinsic optical signal imaging of wild-type and mutant mouse retinas," *Opt. Express* **20**(7), 7646–7654 (2012).
11. C. Li et al., "Distance regularized level set evolution and its application to image segmentation," *IEEE Trans. Image Process.* **19**(12), 3243–3254 (2010).
12. M. J. Rust, M. Bates, and X. Zhuang, "Sub-diffraction-limit imaging by stochastic optical reconstruction microscopy (STORM)," *Nat. Methods* **3**(10), 793–795 (2006).
13. E. Betzig et al., "Imaging intracellular fluorescent proteins at nanometer resolution," *Science* **313**(5793), 1642–1645 (2006).
14. M. F. Juette et al., "Three-dimensional sub-100 nm resolution fluorescence microscopy of thick samples," *Nat. Methods* **5**(6), 527–529 (2008).
15. A. J. Hii et al., "Fast normalized cross correlation for motion tracking using basis functions," *Comput. Methods Programs Biomed.* **82**(2), 144–156 (2006).
16. Q. X. Zhang et al., "In vivo confocal intrinsic optical signal identification of localized retinal dysfunction," *Invest. Ophthalmol. Vis. Sci.* **53**(13), 8139–8145 (2012).
17. L. D. Carter-Dawson and M. M. LaVail, "Rods and cones in the mouse retina. I. Structural analysis using light and electron microscopy," *J. Comp. Neurol.* **188**(2), 245–262 (1979).
18. D. Mustafi, A. H. Engel, and K. Palczewski, "Structure of cone photoreceptors," *Prog. Retinal Eye Res.* **28**(4), 289–302 (2009).
19. C. J. Jeon, E. Strettoi, and R. H. Masland, "The major cell populations of the mouse retina," *J. Neurosci.* **18**(21), 8936–8946 (1998).
20. H. S. Smallman, D. I. A. MacLeod, and P. Doyle, "Vision: realignment of cones after cataract removal," *Nature* **412**(6847), 604–605 (2001).
21. F. S. Werblin and J. E. Dowling, "Organization of the retina of the mudpuppy, *Necturus maculosus*. II. Intracellular recording," *J. Neurophysiol.* **32**(3), 339–355 (1969).
22. D. A. Baylor, M. G. Fuortes, and P. M. O'Bryan, "Receptive fields of cones in the retina of the turtle," *J. Physiol.* **214**(2), 265–294 (1971).
23. D. S. Lebedev and D. W. Marshak, "Amacrine cell contributions to red-green color opponency in central primate retina: a model study," *Vis. Neurosci.* **24**(4), 535–547 (2007).
24. E. A. Rossi et al., "Imaging retinal mosaics in the living eye," *Eye* **25**(3), 301–308 (2011).
25. D. Merino et al., "Observation of cone and rod photoreceptors in normal subjects and patients using a new generation adaptive optics scanning laser ophthalmoscope," *Biomed. Opt. Express* **2**(8), 2189–2201 (2011).
26. N. Doble et al., "In vivo imaging of the human rod photoreceptor mosaic," *Opt. Lett.* **36**(1), 31–33 (2011).
27. C. Owsley et al., "Delays in rod-mediated dark adaptation in early age-related maculopathy," *Ophthalmology* **108**(7), 1196–1202 (2001).
28. R. Klein et al., "The relationship of age-related maculopathy, cataract, and glaucoma to visual acuity," *Invest. Ophthalmol. Vis. Sci.* **36**(1), 182–191 (1995).
29. J. Siderov and A. L. Tiu, "Variability of measurements of visual acuity in a large eye clinic," *Acta Ophthalmol. Scand.* **77**(6), 673–676 (1999).
30. A. Loewenstein et al., "Replacing the Amsler grid: a new method for monitoring patients with age-related macular degeneration," *Ophthalmology* **110**(5), 966–970 (2003).
31. A. Binns and T. H. Margrain, "Development of a technique for recording the focal rod ERG," *Ophthalmic Physiol. Opt.* **26**(1), 71–79 (2006).
32. B. M. Salzberg, A. L. Obaid, and H. Gainer, "Large and rapid changes in light scattering accompany secretion by nerve terminals in the mammalian neurohypophysis," *J. Gen. Physiol.* **86**(3), 395–411 (1985).
33. R. A. Stepanoski et al., "Noninvasive detection of changes in membrane potential in cultured neurons by light scattering," *Proc. Natl. Acad. Sci. U.S.A.* **88**(21), 9382–9386 (1991).
34. H. Kuhn et al., "Interactions between photoexcited rhodopsin and GTP-binding protein: kinetic and stoichiometric analyses from light-scattering changes," *Proc. Natl. Acad. Sci. U.S.A.* **78**(11), 6873–6877 (1981).
35. K. P. Hofmann et al., "Measurements on fast light-induced light-scattering and -absorption changes in outer segments of vertebrate light sensitive rod cells," *Biophys. Struct. Mech.* **2**(1), 61–77 (1976).
36. I. Tasaki and P. M. Byrne, "Rapid structural changes in nerve fibers evoked by electric current pulses," *Biochem. Biophys. Res. Commun.* **188**(2), 559–564 (1992).